Characteristics of cavity solitons and drifting excitations in broad-area vertical-cavity surface-emitting lasers with frequency-selective feedback

Y. Tanguy, N. Radwell, and T. Ackemann*
SUPA, Department of Physics, University of Strathclyde, 107 Rottenrow, Glasgow G4 ONG, Scotland, United Kingdom

R. Jäger
ULM Photonics, Lise-Meitner-Strasse 13, 89081 Ulm, Germany
(Received 17 June 2008; published 6 August 2008)

The properties of cavity solitons in a vertical-cavity surface-emitting laser with frequency-selective feedback from a diffraction grating are characterized and analyzed. The solitons have a typical width of 10 μm and a linewidth of down to 10 MHz, i.e., they represent small microlasers. Their equilibrium spatial location arises from an interplay of spatial inhomogeneities in the device and a grating-induced force which depends on detuning. Transients involve the passage through a self-pulsing state. Due to the grating-induced advection, drifting excitations are found, which might have applications in all-optical delay lines though their solitonic nature remains to be established.

DOI: 10.1103/PhysRevA.78.023810 PACS number(s): 42.55.Px, 42.65.Tg, 42.65.Pc, 42.79.Ta

I. INTRODUCTION

Cavity solitons (CSs) are bistable spatially self-localized waves which exist in the transverse aperture of broad-area nonlinear optical resonators (see, e.g., [1–3]). They are discussed as the basis for future all-optical and potentially massively processing schemes [1,4–6], especially if realized in quite fast, compact, and robust systems as semiconductor microcavities [6–8]. Until recently, most efforts concentrated on systems driven by a coherent beam of high temporal and spatial coherence (the so-called holding beam) using both passive (i.e., absorbing [9]) and active (i.e., amplifying [6,8]) media. Above threshold, CSs have been demonstrated in lasers with an injected signal [10,11]. In all these cases, the frequency and phase of the CSs is locked to that of the injected field, and hence the switch-on and switch-off with an external writing beam is phase sensitive, i.e., demands phase control between the holding beam and the writing beam. This—as well as the very fact that an optical beam of high coherence is needed—is not desirable in applications.

In contrast, a free-running *laser* does not need a coherent holding beam and operates solely from an inexpensive, incoherent source. Hence a *cavity soliton laser (CSL)*, i.e., a laser sustaining CSs, would be beneficial. Unfortunately, the transition from the nonlasing to the lasing state in a normal laser is continuous (supercritical) whereas CSs appear usually only in situations with some form of bistability or multistability between states (see, e.g., the contributions in [3]). CSL where bistability is induced by saturable absorption using dyes or photorefractives as gain medium were reported before [12–15]. More recently, the possibility of CSs in semiconductor lasers with saturable absorbers was pointed out [16]. Guided by reports on bistability in lasers operating in fundamental transverse modes (e.g., [17]), we demonstrated recently an electrically pumped semiconductor CSL based on vertical-cavity surface-emitting lasers (VCSELs) with frequency-selective feedback from a diffraction grating [18,19]. The possibility of self-localization in these devices is supported by recent theoretical analysis of a simplified model [20,21]. Phase-insensitive control of switch-on and switch-off of CSs was demonstrated with switching times down to the tens of nanosecond range (limited by our equipment) [18,19].

In this contribution, we give a detailed experimental characterization of the CSs (Secs. II and III) and especially elucidate on a particular interesting feature stemming from the fact that laser CSs have the freedom to choose different frequencies. CSs of different frequency experience different wave-front tilt and go to slightly different equilibrium positions within the laser aperture (Sec. IV). This effect proves also to be important to understand the switch-on behavior of CSs (Secs. V and VI). It also provides an intrinsic mechanism for *drift* (Sec. VII). The question of a spontaneous drift is interesting from a fundamental point of view [15,22–24] as well as for applications in all-optical processing (e.g., all-optical delay lines) [5,25–27].

II. EXPERIMENTAL SETUP

The experimental setup is similar to the ones described in [18,19], but enhanced for the possibility of following the dynamics with some spatial resolution. It is shown in Fig. 1. The broad-area bottom-emitting VCSELs used have a structure comparable to those in [28], emit at 980 nm, and are electrically pumped through a 200 μm circular oxide aperture. The frequency-selective feedback is provided by a diffraction grating in a Littrow configuration and a self-imaging two-lens system (depicted in Fig. 1). In some experiments, a Littman configuration was used in which the plane of the grating was again imaged with a two-lens telescope onto a highly reflective mirror closing the cavity. This scheme is considerably more complex to align and has higher losses but has a higher frequency dispersion on the other hand.

The VCSEL is operated in the amplifying regime, below its solitary threshold. Due to the strong anisotropy in the

*thorsten.ackemann@strath.ac.uk

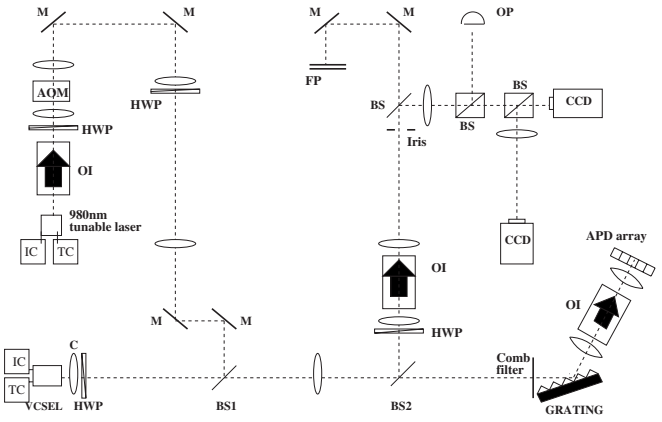

FIG. 1. Experimental apparatus. The self-imaging external cavity is 62 cm long and consists of a 8 mm aspherical lens (C), a 300 mm lens and a holographic grating (1800 lines/mm). One beam sampler (BS2) is inserted to couple out part of the beam for detection (HWP: half-wave plates, OI: optical isolator, M: mirror, BS: beam sampler or beam splitter, CCD: cameras to monitor near and far-field intensity distributions, OP: photodiode to monitor the total optical power, FP: scanning Fabry-Perot). At the position of the iris the near field is reimaged, enabling spatially resolved detection if desired. BS1 is used to allow the writing beam into the cavity (AOM: acousto-optic modulator). Another detection branch uses the zeroth-order reflection of the grating, where an array of APDs was positioned for investigating spatiotemporal dynamics. Also, a comb filter is positioned as close as possible to the reimaged near field at the grating. Both the VCSEL and tunable source are temperature controlled. When the Littman configuration is used, two 100 mm lenses and a highly reflective mirror are added after the grating, which is realigned to a larger angle of incidence.

diffraction efficiency of the grating, the system lases in the horizontal polarization. Two beam samplers are inserted into the external cavity, one is used to pick up a fraction of the beam for detection purposes, while the other allows an external field from a tunable laser source to be injected into the VCSEL, to serve as a writing beam (WB). This WB can be temporally modulated with an acousto-optic modulator (AOM) used as a pulse picker, with a rise and fall time limited to about 15 ns. An additional detection branch can be used from the zeroth order of the grating, where an array of avalanche photodiodes (APD, 180 MHz bandwidth) is positioned to investigate spatiotemporal dynamics.

Several nominally identical devices from the same wafer were available for our studies yielding similar results. Differences can be attributed to uncontrolled inhomogeneities and parameter fluctuations introduced during growth or the subsequent fabrication steps. Most results reported here are obtained from a single device (referred to as device *A* in the following) which demonstrated the best robustness of CS formation in wide areas of the device before it degraded. The results are supplemented by later measurements from a device referred to as *B*.

III. SPONTANEOUS FORMATION OF CSs

At first, the behavior of the near-field intensity distribution is studied under variation of the electrical injection

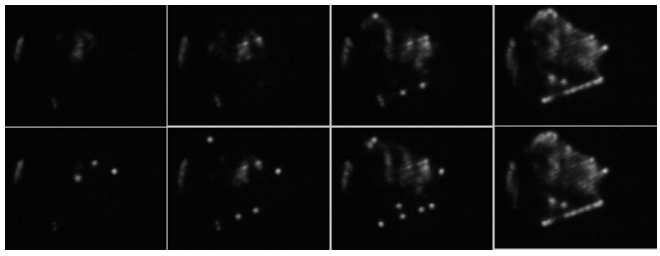

FIG. 2. Near-field intensity distributions with feedback (device *A*). Upper (lower) row: increasing (decreasing) injection current. The bias levels are from left to right: 425.8, 433.7, 443.6, and 459.5 mA. Cavity solitons (CSs) appear preferentially along a defect line in the lower part of the figure, and also on a less discernible defect line at middle height (425.8 mA), although several CSs can also be observed outside these lines.

level. The VCSEL is biased below the threshold of the solitary laser, and the grating is aligned for its frequency to be slightly red detuned with respect to the VCSEL longitudinal resonance frequency. Figure 2 displays near-field intensity distributions when the current is ramped up and down between 400 and 460 mA. For low currents (first picture), only some inhomogeneous optical patterns are occurring; above 430 mA several spontaneously appearing isolated spots are present, which are the CSs. For higher currents (459.5 mA) a spatially extended background pattern becomes more pronounced and the CSs are immersed within it. They become again more discernible with decreasing current, where the bistability of CSs is also evident. For instance, at 425.8 mA three CSs are present, which did not appear at the corresponding current at the ramp-up. Within the bistability range, independent switch-on and switch-off of several CSs by injection of the WB was demonstrated [18,19]. A typical bistability curve for the CS with the lowest threshold is shown in Fig. 5 for reference.

The origin of the bistability can be understood qualitatively by the competition between the two preferred frequencies in the system: the longitudinal resonance of the VCSEL cavity and the frequency where the grating behaves as a perfect retroreflector and the feedback from the external cavity is strongest. We will refer to the latter as "grating frequency" in the following. Initially, they are not aligned; the emission amplitude is low and the carrier density is high. For the same parameter, there might be a state though, in which the emission amplitude is high and the carrier density is low as a consequence. Due to phase-amplitude coupling typical for semiconductor lasers [29], the refractive index increases and hence the wavelength of the cavity resonance is redshifted. This closes a feedback loop and the two resonances are roughly aligned in the upper state of the bistability loop. A detailed treatment of this effect for small-area laser is given in [17,30]. Note that—though nominally it is the current, which is scanned—in effect the x axis in Fig. 5 corresponds also to a wavelength axis due to the increase in resonance wavelength of the VCSEL due to ohmic heating [17,30]. This can be shown by changing the grating frequency (or the bias temperature of the VCSEL) and comparing the thermal wavelength shift expected from the difference in threshold current with the induced wavelength shift (Fig. 3 of [31]

gives a quantitative investigation for a small-area VCSEL). This "parasitic" dispersive effect of the current change dominates the gain effect, at least for high enough currents. Obviously, there is a limit to this regime at low current because at some point the gain is too low for nonlinear effects.

Looking at the emergent structures and arrangements of CSs in more detail, a bright line is clearly apparent at 459.5 and 443.6 mA in the lower part of the near field, which seems to attract and trap CSs. This line presumably originates from strain defects in the active layer. Another defect line, parallel to the previous one but less clearly observable, is present in the midheight of the near field. The CSs appear preferentially along these lines, although we note several CSs appearing in different regions. On the left side of the aperture, there is a region which never lases (neither with CSs nor with extended patterns). In other devices, different configurations of bright and dark defects and CSs are found. These observations provide evidence for inhomogeneities limiting the existence of CSs to certain regions and pinning them at certain locations. The obvious origins of these inhomogeneities are carrier density and temperature inhomogeneities in the active layer and growth inhomogeneities in the spacer layers and Bragg mirrors.

The near-field and far-field intensity distributions of a single CS are shown in Fig. 3. The CS has a full width at half maximum (FWHM) of about 10 μm in the near field, and 2.5° in the far field, which is indistinguishable from the diffraction limit with the resolution available. CSs in VCSELs with injection have a similar size [6]. Their area is some times the diffraction parameter (about 20 μm^2 for our VCSEL) determining the minimal area coupled by diffraction [32].

The determination of the center of the far field is actually not trivial because device *A* was never lasing without feedback and hence there is no reference axis easily available. Device *B* shows off-axis emission from the free-running lasers at low temperatures (about 15 °C), but it shows irregular distortions from rotational symmetry and hence the axis is difficult to define unambiguously. Another method to check the optical axis is tuning the grating frequency. At sufficiently high detuning, off-axis states with a high degree of rotational symmetry are excited, but the axis might change slightly with tuning due to mechanical limitations of the setup. However, comparing the two approaches can give an indication of the uncertainties involved. It is found that the center of the far-field distributions determined by the two approaches agree to within 37% of the angular CS width (i.e., within 1°). The central axis of the CS agrees with the optical axis of the free-running laser within 25% of the CS width and with the one of the feedback-induced far-field ring within 31%. Hence, we conclude that the CSs are located on the optical axis within experimental uncertainty. This agrees with recent theoretical findings [21].

Measurements with a scanning Fabry-Perot interferometer indicate that a CS can operate on a single or multiple longitudinal modes (cf. Fig. 4) of the external cavity, depending on parameters such as current and temperature. This is reasonable since both parameters influence the feedback phase. The behavior resembles the well-known longitudinal mode competition in edge-emitting lasers [33,34]. Even in multi-

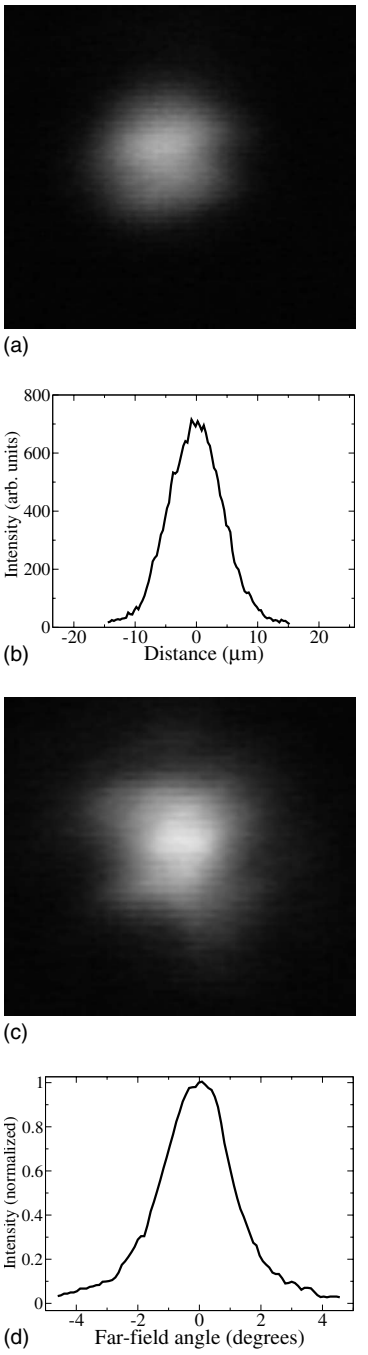

FIG. 3. Near-field (a) and far-field (c) intensity distribution of a CS in device *A* and associated transverse profiles through their center (b, d).

longitudinal mode operation we do not see a pronounced peak at the cavity round-trip frequency in the radio-frequency spectrum. This hints to antiphase behavior between different longitudinal modes [35]. The linewidth of a single mode is 10 MHz, as measured with a Fabry-Perot interferometer with a higher resolution (1 GHz free spectral range). Hence, these bright spots emit coherent radiation, i.e., they are self-sustained microlasers.

We note the presence of inhomogeneous extended emission patterns in the near field, probably stemming from the finite bandwidth of the feedback. They are blue detuned to

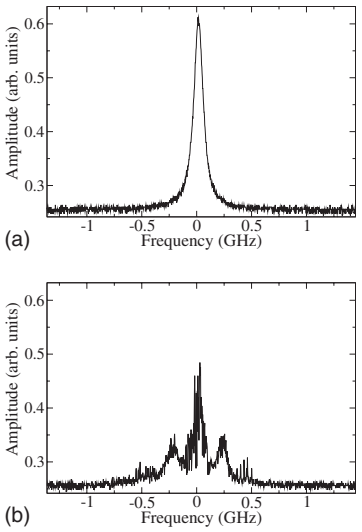

FIG. 4. Optical spectra of a CS, recorded from a confocal Fabry-Perot (10 GHz free spectral range). Depending on parameters such as current and temperature, CSs can operate either in single (a) or multi (b) longitudinal mode operation, separated by the round-trip frequency of the external cavity (240 MHz in the Littrow configuration).

the CS by some tens of GHz and have a much larger linewidth [being essentially flat in the Fabry-Perot (FP) spectrum]. These slightly off-axis patterns hinder the formation of CSs. As reported in [18], spatial filtering of the near field with a comblike filter greatly reduces these patterns. As a result more CSs can appear [18]. (This filter allows feedback only on several horizontal stripes with width 16 μm at the VCSEL, spaced by the same distance.) In the experiments reported in the following, a filter of this kind is used.

Figure 5 shows the dependence of the hysteresis loops on the feedback level. It is evident that the threshold increases, the amplitude of the abrupt jump decreases, and the width of the loop decreases for the decreasing feedback level. The setup can tolerate about 30% more round-trip losses before bistability is lost. This might be used to increase the output power by increasing the current output coupling, which is optimized for flexibility and robustness of operation rather than output power. The current power level is 18 μW in the zeroth order of the grating and 4.5 μW at the intracavity beam splitters, if the polarization is adjusted to be horizontal, and 35 μW, if the polarization is adjusted to be vertical. Hence, closing unnecessary loopholes and using an outcoupler of about 15% transmission, a power level of about 50 μW can be estimated. Further potential for optimization is given by a suitable design of the output coupler of the VCSEL. In addition, there is always the possibility to amplify the pulses before cascading.

IV. DEPENDENCE OF SPATIAL POSITION OF CSs ON CURRENT

Close observation of the CSs reveals that they spatially shift if the current is changed. The CS move to the right of the near field with increasing current (Fig. 6) and to the left

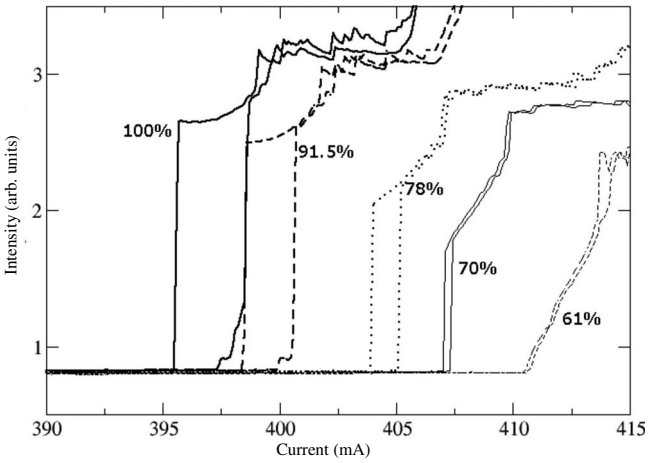

FIG. 5. Hysteresis loops obtained if the injection current is scanned up and down in steps of 0.1 mA at time intervals of 1 s. In the setup of Fig. 1, the half-wave plates are oriented such that the outcoupling losses are minimal for horizontal polarization. The feedback level is attenuated using an additional combination of horizontally oriented linear polarizers with a half-wave plate in between, which is inserted between the second lens and the diffraction grating. The leftmost curve (labeled 100%) is obtained if the half-wave plate is oriented for minimal losses (giving about 86% feedback efficiency). For the other curves, the transmission after a round-trip calculated from Malus' law is indicated. The displacements between the up and the down curves for higher current (after the abrupt switch-on) is mainly due to the fact that different external cavity modes are visited (see also [17]). The offset from zero is due to spontaneous emission (Device B, $T=60$ °C).

with decreasing current, when the grating is oriented as in the right part of Fig. 8. When the direction of the grating is reversed, the direction of the shift is also reversed for all CSs. We stress that this excludes effects inherent to the VCSEL, such as a frequency or carrier gradient across the aperture, as the dominant effect. This phenomenon was already qualitatively explained in Ref. [18] as being the result of attraction between near-field inhomogeneities and a current dependent phase gradient. We give the supporting observations and a more detailed treatment here.

The external cavity can be analyzed with the formalism of *ABCDEF* matrices [36], which allows for optical elements with angular dispersion. In our Littrow configuration, the angular dispersion was calculated to be 0.46 mrad/GHz, i.e., the angular tilt of the fed back beam is changed by 0.46 mrad for every GHz of detuning from the grating frequency. Note that due to the self-imaging geometry, the returning beams are still fed back to the original position but at a slightly different angle from its emission. This does not inhibit feedback since the angular acceptance of the VCSEL resonance (about 26 mrad, estimated from the Bragg mirror reflectivities) is considerably higher than this tilt. In fact, the angular far-field width of a CS, typically 44 mrad (see above), is also much larger, which makes experimental measurement of the tilt quite difficult.

It is very well known that a wave-front tilt leads to a (non-Newtonian) force onto the CS [5,24,37]. In an otherwise homogenous system, it will react by a drift. If the CS—

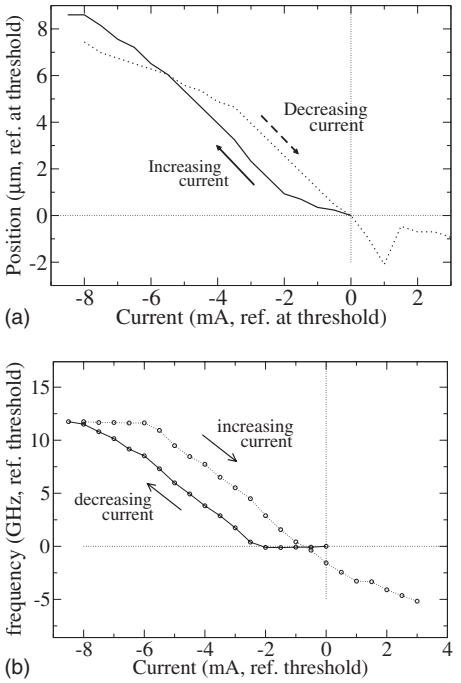

FIG. 6. (a) An example of the relocation of a CS for increasing and decreasing current, and (b) the associated frequency shift. The zero references for position, frequency, and current are taken at the threshold for the spontaneous appearance of the CS (Device *A*).

without the grating-induced tilt—is in the minimum of a trapping potential of a material-induced defect, we expect that it is shifted out of the trapping minimum into a new equilibrium position where the gradients due to the material and due to the grating compensate (possibly it might also leave the trap, if the latter is too shallow).

Figure 6 displays the corresponding measurements. The bottom part shows the change in optical frequency due to the variation of current. The frequency decreases with increasing current, which is expected for a temperature rise due to the Joule heating effect. Obviously, there are small nonlinear feedback effects in addition because there is a small but measurable hysteresis. The upper part shows the dependence of the position of the CS on current. It varies approximately linearly with current and hence with frequency though the frequencies and positions are not entirely correlated. The details of these deviations are not understood.

Figure 7 shows the spatial range over which the CS moves, for both grating orientations. This picture is an addition of several images of a CS obtained by recording the range of CS locations with varying currents, then reversing the grating and reiterating the measurements. The spatial existence ranges are different for the two orientations of the grating. For one orientation, the CS moves from the left to right with increasing current; for the other the CS moves from the right to the left. This is expected since, as the direction of the phase gradient is changed when the grating is reversed, the CS position with regard to the attracting near-field inhomogeneities should also be reversed and the direction of shift should be reversed. It is reasonable to assume that the defect is located in between these spatial ranges. Moreover, as the spatial ranges of existence do not overlap,

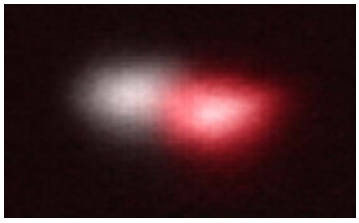

FIG. 7. (Color online) Sum of several near-field images, showing the extent of the CS spatial shift with current variation. The gray and red areas correspond to the two different grating orientations, as shown in Fig. 8. The attracting defect is supposedly located in between these spatial ranges. Two other CSs were investigated, displaying a similar behavior.

the sign of the phase gradient and hence of the detuning should be constant, otherwise the CS would move to both sides of the defect for the same grating orientation. From the fact that the CS moves closer to the defect with increasing current and decreasing frequency, one concludes that the absolute value of the phase gradients becomes smaller for a redshift. This implies that the CS is always blue detuned with respect to the grating frequency. Hence, this allows us to determine indirectly the grating frequency, which is difficult to determine directly with a precision on the GHz level because it depends sensitively on the orientation of the grating.

Obviously, it would be useful to compare these observations to theoretical calculations, but unfortunately the presently available models [20,21] do not allow for the description of the grating-induced wave-front tilt.

V. SWITCHING OF CSs WITH A WB INJECTED ON THE SIDE

The writing and erasure of CSs, with a WB directly on top of the CS location, have been studied in our system in [19]. However, there are also some interesting effects when the WB is positioned on the side of the CS, which are again linked to the geometry of the external cavity and the grating. When the CS exists, injecting the WB on the side usually erases it, except in the specific area where the position of the WB is "upstream" to the final position of the CS with respect to the grating-induced phase gradient. In this case the WB can ignite the CS from the side under appropriate conditions. This is summarized in Fig. 8. Such a behavior is consistent with the trap model in conjunction with the grating-induced phase shift.

It is interesting to investigate whether the WB creates a CS at the injection point, which is drifting into the trap, or whether the WB induces only another perturbation, which is advected towards the trap and then ignited the CS there. For this purpose, the APD array was positioned in an image plane of the near field in the detection branch after the zero order reflection of the grating, allowing one to record the temporal dynamics and also to provide some spatial information. The detectors record the power over area with a width of 7 μm in the near field. The effective separation between two adjacent elements is 11 μm. The resulting data are shown in Fig. 9. The top timetrace displays the WB pulse

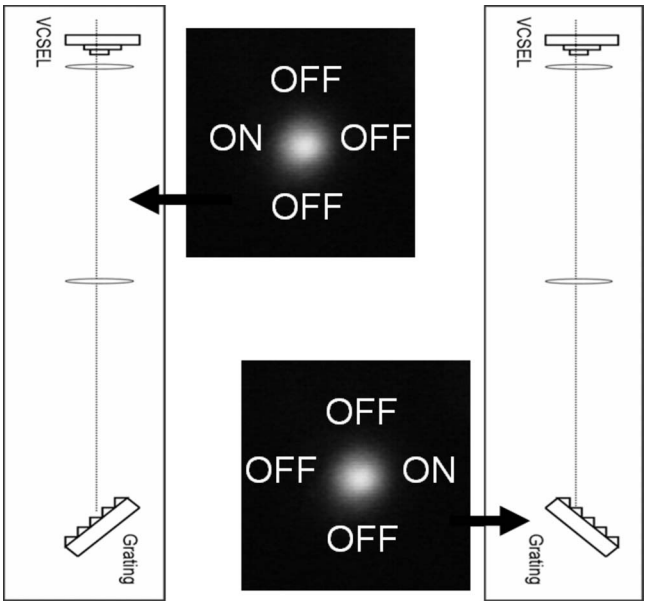

FIG. 8. The two grating orientations and their influence on the switching from a WB injected on the side of the CS. The WB usually erases the CS (as indicated by the "OFF" at these locations), except in the area marked by the "ON." In that region, the CS is excited if the bias current is sufficiently close to the limit point of spontaneous up switching, but will be erased, if the bias current is close to the limit point of spontaneous down switching. The switch-on and switch-off beams are opened and closed mechanically by hand.

(generated by the AOM in this case), while the three others give the response of the system as seen from three consecutive APD elements. The element "3" is located at the WB position, while elements "2" and "1" are the following elements on the left of the near field (the configuration corresponds to the one depicted on the right-hand side of Fig. 8). The main signal is recorded by element 2, which is at the

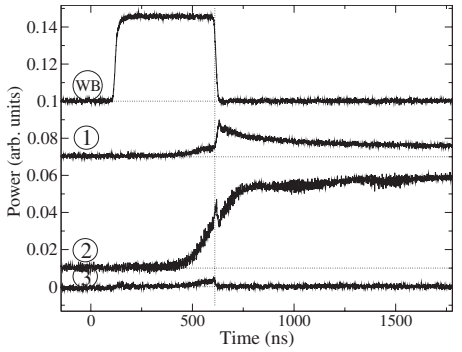

FIG. 9. CS switch-on with a WB injected on the side. The top timetrace shows the pulse from the WB (in the orthogonal polarization), injected on top of the element 3 of the APD array. The other timetraces display the response of the system, with signals from elements 1, 2, and 3. The main signal is observed on element 2, the position of the steady CS. This demonstrates that during the transient the present CS was not switched on directly at the WB position. Timetraces are offset for clarity; a dashed horizontal line indicates the zero in each case.

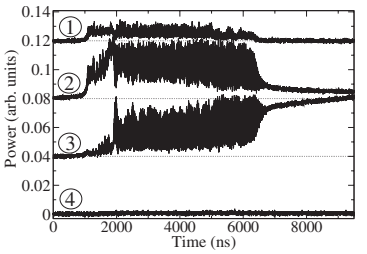

FIG. 10. Typical example for the spatiotemporal dynamics of a CS during spontaneous switch-on. The grating was oriented as in the right panel of Fig. 8 (right), with the element sequence 1 to 4 from left to right. Pronounced pulsations are found over a distance more than two times larger than the CS itself, but only on the elements on top or on the left (downstream) of the stationary CS. Timetraces are offset for clarity, a dashed horizontal line indicates the zero in each case.

location of the stationary CS once the WB is removed, while at the WB position only a small signal is recorded, ending with the blocking of the WB. This shows that the switch-on of the CS actually occurs at the final position of the stationary CS, and probably originates from off-axis emission generated by the WB. Further downstream, a small perturbation can still be seen (element 3) but decays after the writing beam is switched off. The signal observed by element 1 is similar to the behavior observed during a spontaneous switch-on, and will be discussed below. Numerical simulations would be helpful in order to understand the transient better and to comprehend the role of the intermediate off-axis emission, and its unidirectional properties.

VI. SPATIOTEMPORAL DYNAMICS OF SPONTANEOUS SWITCHING

The dynamics of the spontaneous switch-on and switch-off of CSs was investigated. The injection level was set very close to the CS threshold, waiting for perturbations (e.g., small thermal variations, acoustic vibrations, or spontaneous emission noise) to ignite the CS. The spatiotemporal dynamics was recorded by the APD array placed in a near-field image plane. As Fig. 10 shows, pronounced pulsations can occur before the stable lasing state is reached (cf. to trace 3). The pulsing can last for several microseconds. The pulses occur at constant intervals, given by the external cavity round-trip time (see below for a more detailed characterization).

The final, stationary CS is located directly in the center of element 3, however there is also strong pulsing on the adjacent element 2 ("downstream") during the switch-on transient. Measurements, in which the APD array was placed in a far-field imaging plane show that the pulsing states appear slightly off axis (by about 0.5 degrees from the center of the stationary CS), gradually tilting during the transient to reach the emission angle of the stationary CS. This indicates that the signals signal detected on elements 1 and 2 come from a perturbation propagating off axis, in line with the fact that they are downstream with regard to the wave-front tilt. The nature of the transients might be linked to the off-axis pat-

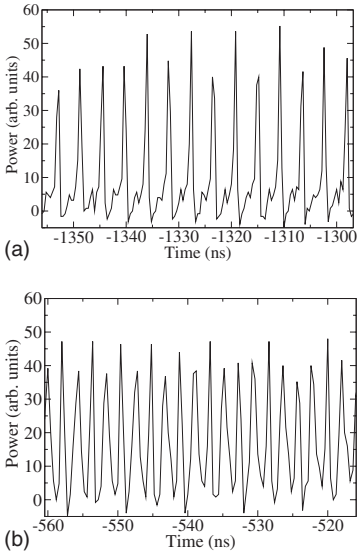

FIG. 11. Close-up of timetraces of a switch-on transient recorded with a fast APD located at the position of the stationary CS (different realization than in Fig. 10). The zero of the time axis is arbitrary. (a) is obtained in the beginning of the transient, (b) later on.

terns observed in the near-field intensity distributions of Fig. 2, as some measurements of their temporal dynamics revealed strongly pulsing dynamics at the cavity round-trip time. A transient through a self-pulsing state at the switch-on of the high-amplitude lasing state is also found in a model for a VCSEL with frequency-selective feedback, which does not include the spatial degrees of freedom [17]. It is due to transient multimode dynamics as different external cavity modes are visited before the final stationary state is reached (see also below). Hence its appearance in the spatially extended system is not surprising.

For a thorough characterization of the dynamics, a higher time resolution than available with the APD array is necessary. Measurements with a faster APD (1.5 GHz bandwidth), but on a single location, are displayed in Fig. 11. The dynamics vary over the time before switch-on, beginning with regularly spaced [every round-trip time (4 ns in this case) Fig. 11(a)] large amplitude pulses. Their amplitude might differ from pulse to pulse. Gradually, additional pulses appear in between two main pulses and the modulation depth decreases [Fig. 11(b)], until the modulation ceased almost completely at the end of the switch-on transient. These dynamics are associated with longitudinal modes, and can be interpreted as a transition to antiphase dynamics [35]. A transition between pulsing and antiphase dynamics is a common scenario in transients of semiconductor lasers with feedback [38,39]. Also in our experiment, CS had typically the most dynamics during their switch-on and switch-off, but were "quiet" (though possibly multilongitudinal mode) in the asymptotic state.

A typical spontaneous switch-off of a CS is displayed in Fig. 12, as monitored by the APD array. The phenomena observed are quite similar to the ones in the switch-on process: Transient pulsed dynamics appears, which is dominated by the cavity round-trip time. Transient dynamics appears

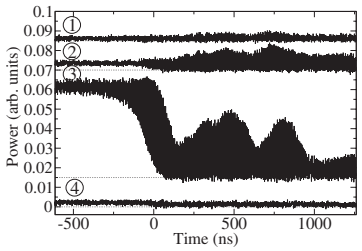

FIG. 12. Spatiotemporal dynamics of a CS spontaneous switch-off. Positioning of elements as in Fig. 10.

also downstream of the CS. Far-field measurements also indicate a gradual off-axis tilt during the transient. This indicates that during the switch-off propagating off-axis structures are excited.

VII. DRAGGING OF THE CS WITH THE WB AND DRIFT PHENOMENA

In this section, we are going to investigate the mobility of a CS and the possibility of a drift. Since the use of the comb filter obviously limits the freedom of motion of a CS, we used the Littman configuration in these experiments. This setup with a four-lens system has a higher frequency selectivity due to the stronger dispersion, and hence reduces the background states without the need for the comb filtering.

The WB (with a polarization orthogonal to the CS) is injected beside the CS, upstream with respect to the phase gradient. When parameters such as the current, frequency, and power of the WB are tuned accordingly, the CS shifts and moves to a location close to the WB, without being erased (Fig. 13). The CS is probably attracted to the WB via the local increase of the refractive index at the WB location, either induced by an increased temperature or a decreased carrier density (via the stimulated emission induced by the WB). Then the CS accompanies any further movement of the WB and can be dragged around, until at a critical distance interaction is lost and the CS returns to its initial position. This demonstrates a high degree of mobility of the CS and illustrates that it is a self-sustained excitation.

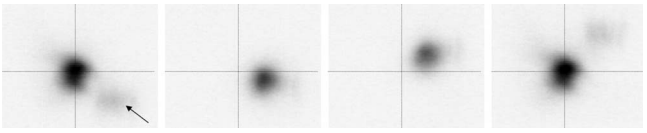

FIG. 13. Shift of CS by a WB. The dark areas correspond to high intensities, vertical and horizontal lines are added for reference. The WB (indicated by an arrow) appears weaker because its polarization is orthogonal to the one of the soliton and this polarization component is attenuated by about a factor of 10 in the detection part. The WB is displaced vertically, moving upwards. The leftmost image shows the CS at its original position, together with the WB (arrow) just before the motion sets in. The CS moves towards the location of the WB, though more on its edge than fully on top of it (second image from the left). It then moves alongside the writing beam (between the second and the third image from the left). In the last picture the CS has moved back to its initial position.

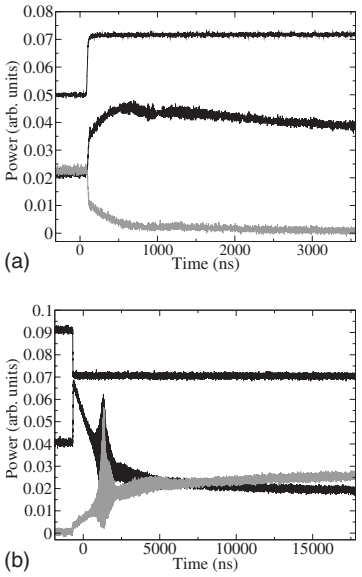

FIG. 14. Spatiotemporal dynamics of the shift of the CS due to the WB. In both panels the top timetrace is the intensity of the WB and is offset for clarity. The two elements of the APD displayed are arranged such that the stationary CS sits just in between, resulting in an equal intensity on both of them. (a) Transient of the shift towards the WB. The dynamics has both a fast and slow component, the fast one following the rise time of the WB, while the CS becomes stationary only after more than 3 μs. (b) Spatiotemporal dynamics after the switch-off of the WB. A fast and slow component of the shift are also observed as well as transient pulsing. We note that the CS did not necessarily move back to its exact initial position.

The transient spatiotemporal dynamics of the CS shift, going towards and from the WB, was investigated with the APD array (Fig. 14). The WB is switched on with the AOM and the resulting evolution of the CS is shown in Fig. 14(a). The shift to the WB contains a fast component, occurring within 25 ns, which is on the order of the rise time of the WB, and a much slower tail, where the CS position stabilizes only after more than 3 μs. These fast and slow time scales are probably associated with carrier dynamics and temperature variations, respectively. We note that the total power of the CS decreases during the shift, which is in line with the decrease of the carrier density at the location of the WB. When the WB is blocked, the CS returns to its original location with similar dynamics [Fig. 14(b)], containing again a fast and a slow component. In addition, transient pulsing occurs. These dynamics resemble those observed during the spontaneous switching sequences. Measurements in the far-field plane showed also that the emission angle is slightly off-axis during these pulses. It might still be self-localized though since the calculation in [20] demonstrates that self-localization can occur in principle for states at all wave numbers.

If the experiment is performed at a lower injection current, the CS not only shifts back to its original location but can continue to drift over relatively large distances (several tens of microns) until it disappears. This behavior was recorded in at least two different areas in the device used,

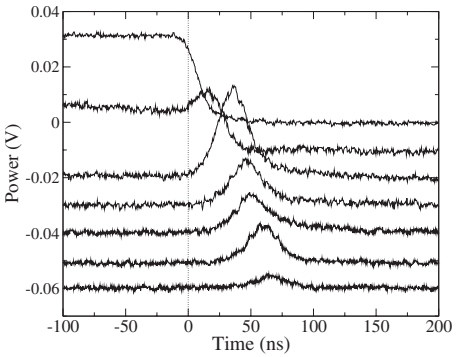

FIG. 15. Spatial drift observed with the elements of the APD array. Initially the CS is ignited by the WB, and is released as soon as the WB is blocked. The timetraces of seven consecutive APD elements are displayed being offset for clarity by 0.02 V. Adjacent elements are spatially separated by 11 μm, so the total drift occurs over a 50 μm length. The amplitude and velocity vary during the propagation. The solitonic nature of the propagating structure is questionable during the drift (see the text).

presumably where the near field is homogeneous enough to support the existence of a CS (or a CS-like excitation) along the path of the drift. Under some circumstances, this drift can also be observed without any preexisting CS, when the WB is applied and switches on a CS which does not remain stationary, once the WB is removed. (The cases of a CS supported by the WB and simply an amplified version of the WB can be distinguished in the optical spectra by the number of peaks. The former one has two peaks: one at the CS frequency and one at the WB frequency.) This is the case for locations at the right-hand (upstream) side of the stationary CS in Fig. 13. Figure 15 presents the timetraces of such a drift, as recorded from seven consecutive elements of the APD array. The drift occurs along a horizontal line over a distance larger than 50 μm. The average velocity is 1.4 μm/ns. The variation of amplitude could be partly the consequence of parameter gradients (or more general variations) along the path.

The behavior in the far field was also monitored with the APD array during this drift. These measurements indicate that the far-field angle of the drifting optical pattern undergoes a continuous tilt during propagation. The angular difference in the far-field centers of mass, between the initial state and after a 50 μm drift, is about 2.5°. This is about the full width at half maximum (FWHM) far-field angle of the CS. This is a significant tilt, and implies that the properties of the drifting state change during the drift. Possibly, it implies that the drifting pattern does not have solitonic properties. This is an alternative explanation to a parameter gradient for the loss in amplitude during the propagation, as a nonsolitonic pattern would be diffracting. However, solitonic properties cannot be excluded since the calculations reported in [20] demonstrate that self-localization can occur in principle for states at all wave numbers. More detailed theoretical and/or experimental investigations are necessary to clarify these issues.

Drifting CSs are interesting from a fundamental point of view, especially if the drift is spontaneous [15,22–24,40].

They can be also used in all-optical delay lines [5,25–27] because the information written by the WB at the first element can be read with a time delay (here about 40 ns) at the last element. A corresponding experiment in a vertical-cavity amplifier with a holding beam was described recently [27]. The drift velocity was slightly higher but of the same order of magnitude. The achieved drift distance and the delay were slightly shorter than described here. However, in order to access the principle scalability in the system investigated here, it is important to know whether the propagating state remains self-localized.

VIII. SUMMARY AND OUTLOOK

In summary, the properties of cavity solitons in a vertical-cavity surface-emitting laser with frequency-selective feedback from a diffraction grating are characterized and analyzed. The solitons have a typical width of 10 μm and a linewidth of down to 10 MHz, i.e., they represent small microlasers emitting radiation of high temporal and spatial coherence. The experiments were performed at 980 nm because VCSEL growth technology is most developed here but there is no principal obstacle to transfer it to other wavelengths, either in the telecommunication range (for advanced processing in all-optical networks) or possibly in the blue range of the spectrum (for reconfigurable optical storage).

Their equilibrium spatial location arises from an interplay of spatial inhomogeneities in the device and a grating-induced force which depends on the detuning between the frequency of the CS and the grating frequency. Transients involve the passage through a self-pulsing state. Due to the grating-induced advection, drifting excitations are found, which might have applications in all-optical delay lines though their solitonic nature remains to be established. Further theoretical investigations would be helpful to clarify this issue. Drift in CSLs might also have peculiar features different from the drift in a driven system, e.g., it was predicted that laser cavity solitons might have inertia, at least in certain situations [15].

In passive devices, the injection angle of the holding beam is used to induce and to control the drift [37]. Since this holding beam is not present in a free-running laser scheme, there is a need to put a gradient of another parameter across the aperture of a CSL to induce a drift. Hence, the fact that the parity is intrinsically broken by the detuning in our system might be a considerable advantage of our grating-based CSL system over other proposed schemes of cavity soliton lasers [16], at least for applications relying on drift.

ACKNOWLEDGMENTS

This work was supported by the European Union within the FunFACS project, a grant by the Faculty of Science of the University of Strathclyde, the EPSRC, and by the Deutsche Forschungsgemeinschaft. We are grateful for useful discussions with W. J. Firth, P. Paulau, N. A. Loiko, and G.-L. Oppo.

[1] W. J. Firth and C. O. Weiss, Opt. Photonics News **13**, 54 (2002).
[2] L. A. Lugiato, IEEE J. Quantum Electron. **39**, 193 (2003).
[3] *Dissipative Solitons*, edited by N. Akhmediev and A. Ankiewicz, Lecture Notes in Physics, Vol. 661 (Springer, New York, 2005).
[4] G. S. McDonald and W. J. Firth, J. Opt. Soc. Am. B **7**, 1328 (1990).
[5] N. N. Rosanov, Proc. SPIE **1840**, 130 (1991).
[6] S. Barland *et al.*, Nature (London) **419**, 699 (2002).
[7] V. B. Taranenko, C. O. Weiss, and B. Schäpers, Phys. Rev. A **65**, 013812 (2001).
[8] S. Barbay, Y. Ménesguen, X. Hachair, L. Leroy, I. Sagnes, and R. Kuszelewicz, Opt. Lett. **31**, 1504 (2006).
[9] V. B. Taranenko and C. O. Weiss, Appl. Phys. B: Lasers Opt. **72**, 893 (2001).
[10] Y. Larionova and C. Weiss, Opt. Express **13**, 10711 (2005).
[11] X. Hachair *et al.*, IEEE J. Sel. Top. Quantum Electron. **12**, 339 (2006).
[12] V. Y. Bazhenov, V. B. Taranenko, and M. V. Vasnetsov, Proc. SPIE **1840**, 183 (1992).
[13] M. Saffman, D. Montgomery, and D. Z. Anderson, Opt. Lett. **19**, 518 (1994).
[14] V. B. Taranenko, K. Staliunas, and C. O. Weiss, Phys. Rev. A **56**, 1582 (1997).
[15] N. N. Rosanov, *Spatial Hysteresis and Optical Natterns*, Springer Series in Synergetics (Springer, Berlin, 2002).
[16] M. Bache, F. Prati, G. Tissoni, R. Kheradmand, L. A. Lugiato, I. Protsenko, and M. Brambilla, Appl. Phys. B: Lasers Opt. **81**, 913 (2005).
[17] A. Naumenko, N. A. Loiko, M. Sondermann, K. F. Jentsch, and T. Ackemann, Opt. Commun. **259**, 823 (2006).
[18] Y. Tanguy, T. Ackemann, W. J. Firth, and R. Jäger, Phys. Rev. Lett. **100**, 013907 (2008).
[19] Y. Tanguy, T. Ackemann, and R. Jäger, Opt. Express **15**, 16773 (2007).
[20] P. V. Paulau, A. J. Scroggie, A. Naumenko, T. Ackemann, N. A. Loiko, and W. J. Firth, Phys. Rev. E **75**, 056208 (2007).
[21] P. V. Paulau, D. Gomila, T. Ackemann, N. A. Loiko, and W. J. Firth, Phys. Rev. E **78**, 016212 (2008).
[22] A. J. Scroggie, J. M. McSloy, and W. J. Firth, Phys. Rev. E **66**, 036607 (2002).
[23] H. U. Bödeker, M. C. Röttger, A. W. Liehr, T. D. Frank, R. Friedrich, and H. G. Purwins, Phys. Rev. E **67**, 056220 (2003).
[24] T. Ackemann and W. J. Firth, in *Dissipative Solitons*, edited by N. Akhmediev and A. Ankiewicz Lecture Notes in Physics, Vol. 661 (Springer, New York, 2005), pp. 55–100.
[25] W. J. Firth, Proc. SPIE **4016**, 388 (2000).
[26] B. Schäpers, T. Ackemann, and W. Lange, Proc. SPIE **4271**, 130 (2001).
[27] F. Pedaci *et al.*, Appl. Phys. Lett. **92**, 011101 (2008).
[28] M. Grabherr, M. Miller, R. Jäger, R. Michalzik, U. Martin, H.

J. Unold, and K. J. Ebeling, IEEE J. Sel. Top. Quantum Electron. **5**, 495 (1999).
[29] C. H. Henry, IEEE J. Quantum Electron. **18**, 259 (1982).
[30] A. V. Naumenko, N. A. Loiko, and T. Ackemann, Phys. Rev. A **76**, 023802 (2007).
[31] A. Naumenko, N. A. Loiko, K. F. Jentsch, and T. Ackemann, Proc. SPIE **6725**, 672522 (2007).
[32] L. Spinelli, G. Tissoni, M. Brambilla, F. Prati, and L. A. Lugiato, Phys. Rev. A **58**, 2542 (1998).
[33] L. A. Coldren and S. W. Corzine, *Diode Lasers and Photonic Integrated Circuits* (Wiley, New York, 1995).
[34] L. Furfaro, F. Pedaci, M. Giudici, X. Hachair, J. Tredicce, and S. Balle, IEEE J. Quantum Electron. **40**, 1365 (2004).
[35] E. A. Viktorov and P. Mandel, Phys. Rev. Lett. **85**, 3157 (2000).
[36] O. E. Martinez, IEEE J. Quantum Electron. **24**, 2530 (1988).
[37] W. J. Firth and A. J. Scroggie, Phys. Rev. Lett. **76**, 1623 (1996).
[38] G. Vaschenko, M. Giudici, J. J. Rocca, C. S. Menoni, J. R. Tredicce, and S. Balle, Phys. Rev. Lett. **81**, 5536 (1998).
[39] M. Sciamanna, T. Erneux, F. Rogister, O. Deparis, P. Mégret, and M. Blondel, Phys. Rev. A **65**, 041801(R) (2002).
[40] S. V. Fedorov, A. G. Vladimirov, G. V. Khodova, and N. N. Rosanov, Phys. Rev. E **61**, 5814 (2000).